Effect of Fin Pitch on Flow and Heat Transfer in Multilouvered Fins

Z. Xiaogang and D. K. Tafti

ACRC TR-150 April 1999

For additional information:

Air Conditioning and Refrigeration Center
University of Illinois
Mechanical & Industrial Engineering Dept.
1206 West Green Street
Urbana, IL 61801

(217) 333-3115

Prepared as part of ACRC Project 94
Computational Study Of Multilouvered Fin Heat Exchangers
D. K. Tafti, Principal Investigator

The Air Conditioning and Refrigeration Center was founded in 1988 with a grant from the estate of Richard W. Kritzer, the founder of Peerless of America Inc. A State of Illinois Technology Challenge Grant helped build the laboratory facilities. The ACRC receives continuing support from the Richard W. Kritzer Endowment and the National Science Foundation. The following organizations have also become sponsors of the Center.

Amana Refrigeration, Inc.
Brazeway, Inc.
Carrier Corporation
Caterpillar, Inc.
Chrysler Corporation
Copeland Corporation
Delphi Harrison Thermal Systems
Frigidaire Company
General Electric Company
Hill PHOENIX
Honeywell, Inc.
Hussmann Corporation
Hydro Aluminum Adrian, Inc.
Indiana Tube Corporation
Lennox International, Inc.
Modine Manufacturing Co.
Peerless of America, Inc.
The Trane Company
Thermo King Corporation
Visteon Automotive Systems
Whirlpool Corporation
York International, Inc.

For additional information:

Air Conditioning & Refrigeration Center
Mechanical & Industrial Engineering Dept.
University of Illinois
1206 West Green Street
Urbana IL 61801

217 333 3115

Submitted: 4th ISHMT/ASME Heat and Mass Transfer Conference, Pune, India, 12-15 January 2000.

EFFECT OF FIN PITCH ON FLOW AND HEAT TRANSFER IN MULTILOUVERED FINS

Zhang Xiaogang
&
Danesh Tafti

National Center for Supercomputing Applications
University of Illinois at Urbana Champaign
Urbana, IL 61801
USA.

ABSTRACT

High resolution time-dependent calculations are performed for developing flow and heat transfer in a multilouvered fin geometry to study the effect of fin pitch. In both cases, transition to unsteadiness occurs in the wake of the exit louver at a Reynolds number of 400. The upstream spatial propagation of instabilities proceeds much faster for the larger fin pitch. It is also found that the nature of instabilities differs between the two fin pitches. For the larger fin pitch, louver wake instabilities play a more dominant role than louver leading edge shear layer instabilities, which dominate the smaller fin pitch. Overall heat transfer increases per fin as the fin pitch increases because of the larger mass flow rate between fins. However, the difference in heat transfer coefficient between the two geometries is small except in the transitional and low Reynolds number range.

INTRODUCTION

The increasing demand for compact heat exchangers in the automotive industry as well as many refrigeration and air-conditioning applications has necessitated the use of various interrupted surfaces to augment air-side heat transfer. One of the most widely used design among interrupted surfaces is the

multilouvered fin geometry. During the past 20 years many experimental studies have attempted to understand the flow phenomena and performance characteristics in louvered fins [1,2,3,4,5]. A number of numerical studies [6,7,8,9] in the steady laminar flow regime have complemented experiments with varying degrees of success. Achaichia et al. [10] studied the flow pattern in multilouvered fins with the commercial code PHOENICS along with the k-ε turbulence model for high Reynolds numbers. However, high Reynolds number turbulence models are not very accurate in the unsteady laminar and low Reynolds number turbulence regimes encountered in compact heat exchangers. Consequently, these models overpredict the friction and heat transfer. On the other hand, low Reynolds number turbulence models [11] can sense the "state" of turbulence in the flow. In spite of this property, these models do not have a high degree of receptivity to transition from laminar to unsteady laminar and to turbulent flow. As pointed out in Zhang et al. [12,13], the large-scale self-sustained flow oscillations, which develop in compact heat exchangers, have considerable impact on the heat transfer and friction factor, and their improper representation can lead to erroneous predictions.

The objective of the current paper is to perform high resolution time-dependent calculations to study the effect of fin pitch on developing flow and heat transfer in multilouvered fin geometries. We study the effect of fin pitch on general flow features, on transition, and on heat transfer and friction.

MATHEMATICAL FORMULATION

To calculate the flow and thermal fields in the array, we map the Navier-Stokes and energy equations from physical to logical/computational space by a boundary conforming transformation. The governing equations for momentum and energy conservation are discretized with a conservative finite-volume formulation. Both convection and viscous terms are approximated by second-order central-difference schemes. The computational domain, consists of one entire row of the louvered fin geometry allowing for the inclusion of entrance and exit effects in the flow direction. Periodic boundary conditions are applied in the transverse direction whereas Dirichlet boundary conditions are specified at

the entrance to the array. To facilitate the calculation of the whole array, we use a structured multi-block formulation in the streamwise direction with overlapping boundaries for the application of inter-block boundary conditions. A downstream block, which does not include any louvered fin, is added to ensure that the fully developed boundary condition can be applied at the exit.

The governing flow and energy equations are non-dimensionalized by a characteristic length given by the louver pitch L_P^*, a characteristic velocity scale given by the inlet velocity to the array (u_{in}^*) and a temperature scale given by $(T_f^* - T_{in}^*)$, where T_f^* is the specified fin surface temperature. The non-dimensionalization results in a characteristic Reynolds number $\mathrm{Re} = \mathrm{Re}_{in} = u_{in}^* L_p^* / \nu$, with Dirichlet boundary conditions $u_{in} = 1, T_{in} = 0$ at the entrance to the computational domain. At the fin surface, no slip, no penetration boundary conditions for the velocity field, and $T_f = 1$ for the temperature field are applied. More details about the time-integration algorithm, treatment of boundary and louver surface conditions, and validation of the computer program can be found in Tafti et al. [14].

GEOMETRY AND COMPUTATIONAL DETAILS

The configuration used in the calculations consists of an entrance and exit louver with four louvers on either side of the center or re-direction louver as shown in Figure 1(a). Table 1 summarizes the non-dimensional geometric parameters; F_p is the fin pitch, θ is the louver angle, and b, the fin thickness. The Reynolds number based on louver pitch and inlet flow velocity is nominally varied from 100 to 1300. Results for two ratios of fin pitches (1 and 1.5) are shown here.

The computational domain is resolved by 15 computational blocks as shown in Figure 1(b), one for each louver, two each for the entrance, exit and re-direction louver, and an exit domain which extends approximately 7.2 non-dimensional units downstream of the exit louver. Although the flow is

nominally two-dimensional the spanwise extent of the domain is unity in non-dimensional terms (L_p^* in dimensional units). In both cases, a total resolution of 138,240 computational cells is used corresponding to 96x96 cells in each computational block. The mesh is clustered and orthogonal in the vicinity of the louvers. Each calculation in the unsteady regime takes about 1000 CPU hours or about 67 hours of wall clock time on 15 processors of a SGI-Cray Origin 2000 system. A grid independency study was performed at a resolution of 128x128 cells in each block (a total of 245,760 cells) for Re_{in} = 1000. The Nusselt number calculated on the 96x96 grid was within *one* percent of the fine grid calculation. All results reported here on the 96x96 grid per block. For the unsteady cases extreme care was taken to ascertain that the flow and heat transfer had reached a stationary state before any time averaged data or frequency data was obtained.

DATA REDUCTION AND PRESENTATION OF RESULTS

In this section we define the relationship between dimensional and non-dimensional parameters used to quantify the heat transfer, pressure drop and friction. The dimensional heat flux on the louver surface is defined as

$$q^* = -k\frac{\partial T^*}{\partial n^*} = h^*(T_f^* - T_{ref}^*) \tag{1}$$

where n^* is measured along the normal to the louver surface, and T_{ref}^* is a reference temperature. Rewriting equation (1) we can define the non-dimensional heat flux and Nusselt number as

$$Nu = \frac{h^* L_p^*}{k} = \frac{-\partial T/\partial n}{(1-T_{ref})} \quad \text{and} \quad q = \frac{q^* L_p^*}{k(T_f^* - T_{in}^*)} = -\frac{\partial T}{\partial n} \tag{2}$$

When $T_{ref} = T_{in} = 0$, we define a local Nusselt number on the louver surface as

$$Nu^1 = q = -\frac{\partial T}{\partial n} \tag{3}$$

We further define an average Nusselt number on each louver, $< Nu^1 >_{louv}$, and for the whole multilouvered fin, $< Nu^1 >_{fin}$. We note that for $T_{ref} = T_{in}$, the calculated Nusselt number is representative of the non-dimensional local, or the average heat flux.

We further define a Nusselt number based on the mixed mean temperature given by

$$Nu^2 = \frac{h^* L_p^*}{k} = \frac{-\partial T / \partial n}{(1 - T_{ref})}, \text{ where } T_{ref} = T_{mean} = \frac{\sum_{F_p} |u| T \Delta y}{\sum_{F_p} |u| \Delta y} \tag{4}$$

Based on the above definition we define two additional Nusselt numbers, one for each individual louver, $< Nu^2 >_{louv}$, and the other for the whole multilouvered fin, $< Nu^2 >_{fin}$. For the former, T_{mean} is calculated in the computational block or blocks surrounding the louver, and in the latter T_{mean} is calculated for the whole multilouvered fin (based on the flow depth F_d). We define the Colburn factor as:

$$j = \frac{< Nu^2 >_{fin}}{\mathrm{Re}_L \, \mathrm{Pr}^{0.4}} \tag{5}$$

where $\mathrm{Re}_L = V_c^* L_p^* / \nu = V_c \, \mathrm{Re}_{in}$, and V_c^* is the mean flow velocity at the minimum flow cross-sectional area, A_c^*.

The friction factor f, is defined as

$$f = \frac{2(\Delta P_{fin}^*) D_h^*}{4 \rho L_{x1}^* V_c^{*2}} = \frac{2(\Delta p_{fin} / (F_p \cdot 1)) D_h}{4 L_{x1} V_c^{\ 2}} \tag{6}$$

where $D_h^* = \frac{4A_c^*}{\Omega_{fin}^* / L_{x1}^*}$, where A_c^* is the minimum cross-sectional flow area and Ω_{fin}^* is the total fin surface area. In addition we also calculate the pressure force due to form drag on a louver by louver basis as follows:

$$\Delta p_{louv}^{form} = \sum_{\Omega_f} P\vec{n} \cdot \vec{e}_x \partial\Omega_{louv} , \tag{7}$$

where $\vec{n}$ is the unit normal to the louver surface and $\vec{e}_x$ is the unit vector in the x direction.

RESULTS

Effect of Fin Pitch on General Flow Features

Figure 2 shows a schematic of the general flow features observed in the louvered array during the steady laminar regime up to a Reynolds number of 400. At Re_{in} = 400 the wake of the exit louver develops instabilities and the flow becomes unsteady. For both fin pitches, recirculation regions are observed in the wakes of louvers at Re_{in} = 100. These grow as the Reynolds number increases. For the larger fin pitch, the leading edge shear layers separate and reattach to form recirculation regions on the top surface of louver 2 and the bottom surface of louver 7 by Re_{in} = 200. These recirculation regions appear at Re_{in} = 300 for the smaller fin pitch. Both the re-direction louver and the exit louver also develop recirculation regions by Re_{in} = 200. In general, separation and reattachment occurs earlier for the larger fin pitch .

Previous research [3,4,5] has shown that there are two asymptotic flow regimes which exist in multilouvered geometries. The "duct" flow regime is when the flow is directed in the axial direction

between fins, and "louver directed", when the bulk of the flow is directed in the louver direction. The former is associated with low heat transfer, whereas the latter with high heat transfer. The existence of these flow regimes is dependent on the geometry and Reynolds number.

An important parameter, which is used to quantify the flow regime is the "flow efficiency", which is defined as the degree to which the flow is aligned to the louver direction [4]. In order to quantify this effect in our numerical calculations, we define a mean flow angle for *each louver* as follows:

$$\alpha = \tan^{-1}\left(\frac{v_{avg}}{u_{avg}}\right) \tag{8}$$

The numerator is the average y-flow velocity calculated on the top boundary of the computational block, and the denominator is the average x-flow velocity calculated at the left or incoming boundary of the block. Figure 3 plots the calculated flow angles (time mean in the unsteady regime) for the two fin pitches for louvers on either side of the redirection louver at Re_{in} = 100, 400, 800, and 1200. For F_p = 1.0, the flow is very nearly louver directed with α varying between 26 and 30 degrees. The flow direction has reached a near asymptotic state by Re_{in} = 400. For F_p = 1.5, the flow angle varies between 20 to 28 degrees as it moves into the array and as the Reynolds number increases. A near asymptotic state has been reached by Re_{in} = 800.

Effect of Fin Pitch on Transition

In Tafti et al. [15], three possible mechanisms were identified which could potentially contribute to transition in the multilouvered flow geometry: a wake instability [16], which is characterized by the classical Von Karman vortex street [17]; a Kelvin-Helmholtz instability or free-shear-layer instability as

observed in leading edge separation and reattachment in flow over blunt flat plates [18,19]; and finally, a impinging shear-layer instability (ISLI) as observed in the vortex shedding from elongated rectangular cylinders [20,21,22].

Tafti et al. [15] have performed a detailed study of transition for F_p =1.0. It was found that a wake instability developed at the exit louver at Re_{in} = 400, which gradually spread upstream into the louvered array. Figure 4 shows instantaneous vorticity contours for the two fin pitches at three representative Reynolds numbers. For F_p = 1.0, it was found that the initial wake instability moved inside the array and excited a leading edge shear layer or Kelvin-Helmholtz instability at the louvers near the exit. By Re_{in} = 1000, there was clear evidence of leading edge vortices being shed on all louvers in the downstream half of the array. As the Reynolds number increased, the leading edge instability moved further upstream into the array and by Re_{in} = 1300, all louvers exhibited leading edge vortex shedding with the exception of the entrance and the first two louvers. During this process, there was a single characteristic frequency observed at all spatial locations (irrespective of whether vortex shedding was present or not) at a given Reynolds number inside the array. With the exception of Re_{in} = 800, the characteristic frequency inside the array was usually equal to the first harmonic of the exit wake instability.

For F_p = 1.5, the initial instability is also found to occur in the wake of the exit louver at Re_{in} = 400 as shown in Figure 4. The observed characteristic wake frequency had a value of f = 0.73 versus 0.84 for F_p = 1.0. However, for F_p = 1.5 the instability moved upstream into the array much faster than for F_p = 1.0. For example, by Re_{in} = 700, the wakes of louvers in the downstream half of the array exhibit a wavy unstable character with considerable evidence of unsteadiness as these wakes impinge on downstream louvers. By Re_{in} = 800, the exit and redirection louver show vortex shedding from the leading edges, while there is considerable wake unsteadiness behind each louver throughout the array,

which in turn destabilize the leading edge shear layers as they impinge on downstream louvers. Similar to F_p = 1.0, each Reynolds number is characterized by a single dominant frequency inside the array. However, unlike F_p =1.0, the dominant frequency inside the array is not always in tune with the exit wake frequencies. For F_p =1.5, once the exit wake instability appears at Re_{in} = 400, there is evidence of infiltration of the exit wake frequency at louvers near the exit at Re_{in} = 500 and 600. Between Re_{in} = 700 and 900, the interior of the array is characterized by a frequency near 1.26, while the exit wake still maintains a characteristic frequency between 0.7-0.8 with a first harmonic between 1.4-1.6. Between Re_{in} = 1000 and 1200, the spectra in the exit wake and the interior of the louvered array (particularly the downstream half) become broad banded with no clear peaks. In this range there is evidence of a low frequency component (0.7) with a first harmonic at (1.4) developing in the interior. These peaks are quite well defined in the upstream half of the array at Re_{in} = 1000, but become broad-banded as the Reynolds number increases to Re_{in} =1200. It is conjectured that during this range of Reynolds numbers the flow undergoes a transition to a different mode of unsteadiness. When the Reynolds number is increased to 1300, there is a complete shift in the unsteady character of the flow. The time signals now become much more ordered with well-defined spectral peaks. More importantly, the characteristic frequency inside the array is now the same as the exit wake frequency of (0.8), with a first harmonic occurring at (1.6). The reason for this behavior is not fully understood at this time.

Effect of Fin Pitch on Heat Transfer

Changing the fin pitch has two counter-acting bulk effects on the heat transfer capability of a single fin. Increasing the fin pitch, increases the effective flow area between two fins. Hence, for the same Reynolds number based on L_p^*, conditions are less favorable for louver directed flow. This is

captured in Figure 3. As the fin pitch increases, the flow angle decreases, hence a smaller percentage of flow passes through the louvers. However, at the same time the overall bulk flow rate between fins increases. The flow situation represented by the simulations is of a heat exchanger with the same frontal area. Depending on the fin pitch, more or less fins can be placed in the heat exchanger and for the same overall mass flow rate, the mass flow between two fins varies. Hence, on one hand, the total mass flow between fins increases, and on the other, the percentage of louver directed flow decreases as the fin pitch increases. The former creates a larger potential for heat transfer, while the latter tends to inhibit heat transfer.

Figure 5 compares the mean temperature fields for the two cases for Re_{in} = 400, 800, and 1000. According to Suga and Aoki. [8], thermal wake interference plays an important role in deciding the heat transfer in a multilouvered fin array. If a downstream louver lies directly in the path of the thermal wake of an upstream louver then the effective heat transfer is reduced due to the reduced temperature potential on the downstream louver. Equation (9) relates geometrical parameters to the wake interference phenomenon by the following relationship:

$$\frac{F_p}{L_p \tan(\theta)} = n. \tag{9}$$

When n is an integer (2, 3...) there is direct wake interference, if n = 2.5, 3.5 then the wake of an upstream louver passes between downstream louvers. Although, equation (9) assumes the wake trajectory is a straight line, which it seldom is, it gives a first order estimate of thermal wake effects. For F_p = 1.5, n = 2.6, whereas for F_p =1.0, n = 1.73 from equation (9). Hence, in Figure 5 for F_p = 1.5, the entrance louver and the first two louvers are free of any thermal wake effects, whereas for F_p =1.0, only the entrance louver and the first louver are free of thermal wake effects. In general it can be concluded that thermal wake interference is much stronger for smaller fin pitches due to the close proximity of louvers.

Figure 6 plots the local distribution of time mean Nu^1 on the top and bottom surfaces of each louver for Re_{in} = 400 and 800. In addition, figure 7 plots the time mean Nusselt number averaged over each louver, $< Nu^1 >_{louv}$, for Re_{in} = 400, 800 and 1000. $< Nu^1 >_{louv}$ has a direct equality with non-dimensional heat flux and includes the effect of decreasing temperature potential as one moves downstream into the array. Hence in general, $< Nu^1 >_{louv}$ decreases in the downstream direction as the temperature potential decreases. We make the following observations from the two figures:

(a) $< Nu^1 >_{louv}$ is higher for the larger fin pitch – this trend is dominated by the increased mass flow rate between the fins and subsequently through the louvers. Therefore, more heat is transferred per fin for the larger fin pitch.

(b) For F_p = 1, there is a sharp drop in the Nusselt number on louvers 3 and 8. This is a direct result of thermal wake interference from the entrance louver (louver 1) and the redirection louver (louver 6), respectively.

(c) For both fin pitches there is a sharp drop in the Nusselt number on the re-direction louver. From the local distribution in Figure 6, there is a sharp decline in Nu^1 on the bottom surface in the region where the louver transitions to the landing. Flow visualization studies show a large recirculating region at this junction on the bottom surface as seen in Figure 2.

(d) From the local distribution in Figure 6, it is clear that larger the flow impingement angle to the louver, the surface on which the flow impinges exhibits much higher heat transfer. This effect is strongest on louver 2 on which the bottom surface has a much higher distribution of Nu^1. Similarly, the top surface of louver 7 exhibits high heat transfer. Flow visualization studies also show recirculation regions at the leading edge on the top surface of louver 2 and bottom surface of louver 7. The difference in heat transfer between the top and bottom surface is much larger for the higher fin pitch due to the larger flow impingement angle.

(e) For the larger fin pitch, F_p =1.5, as the flow enters the louvered array, $< Nu^1 >_{louv}$ increases gradually and maximizes at louver 3 or 4. This is a result of less thermal wake interference contrary to the trend for F_p =1.0. This trend gets more pronounced as the louver angle decreases and the fin pitch increases. The large jump in $< Nu^1 >_{louv}$ observed on louver 9 for Re_{in} = 400 is a result of low temperature freestream fluid entering between louvers 3 and 4, which is then redirected and impinges on louver 9. This effect can be seen in Figure 5.

(f) For F_p =1.5, as the Reynolds number increases to Re_{in} = 800, $< Nu^1 >_{louv}$ in the downstream half of the array show a marked rise in relation to the upstream half. This is a result of the self-sustained flow oscillations which enhance the heat transfer capability of the louvers. The same can be observed for F_p =1.0, albeit at the higher Reynolds number of 1000.

The corresponding louver by louver distribution of the time mean $< Nu^2 >_{louv}$ is shown in Figure 8. The use of the mixed mean temperature as the reference temperature equalizes the mean temperature potential across louvers. In doing so it also nullifies the effect of different mass flow rates between the two fin pitches. Therefore, $< Nu^2 >_{louv}$ accentuates perturbations in the temperature field (about the mixed mean temperature) caused by wake interference effects, vortex shedding and other fluid dynamic phenomenon. This effect can be clearly seen in comparisons of $< Nu^2 >_{louv}$ between the two geometries and also between the upstream and downstream half of the arrays. Once unsteadiness is established in the downstream half of the array, $< Nu^2 >_{louv}$ in the downstream half exhibits values higher than in the upstream half. This trend is observed for $Re_{in} > 800$ for F_p =1.5 and $Re_{in} > 1000$ for F_p =1.0. For Re_{in} = 400 and F_p =1.5, we observe that the Nusselt number is largest on louver 9. In the absence of unsteady motion at this Reynolds number, this result is quite unexpected. However, as noted in (e) above, this is a result of low temperature freestream fluid being directed in the vicinity of the louver. The low

temperature fluid insulates the louver from the surrounding high temperature fluid and enhances heat transfer. This effect combined with a high mixed mean temperature results in a $< Nu^2 >_{louv}$ which is higher than louvers 1 and 2 (see equation (4)).

Figure 9 plots the distribution of time mean $< Nu^1 >_{fin}$ and $< Nu^2 >_{fin}$ versus Reynolds number for the whole fin. $< Nu^1 >_{fin}$ is larger for the larger fin pitch. Hence the total heat transferred is larger for the larger fin pitch over the range of Reynolds numbers. On the other hand, for $< Nu^2 >_{fin}$, which is representative of the heat transfer coefficient, the differences between the two fin pitches are accentuated at low Reynolds numbers and in the region of transition. For Rein < 500, $< Nu^2 >_{fin}$ for F_p = 1.0 is larger than F_p =1.5. The differences get larger as the Reynolds number decreases. This trend is dominated by the larger relative degree of "louvered directed flow" for the smaller fin pitch.

Effect of Fin Pitch on Friction Losses

Pressure losses in a multilouvered array have two main components, form drag and friction drag. Figure 10(a) plots the friction factor *f*, calculated by using equation (6), and for completeness, the *j* factor from equation (5). The friction factor is larger for the smaller fin pitch by about 15%. However, the differences are much larger as the Reynolds number decreases. In both cases, the *f* and *j* factors exhibit a strong sensivity to transition. The *f* factor asymptotes to a near constant value beyond Re_{in} = 1200. Figure 10(b) plots the fractional contribution of form drag to the total pressure loss encountered. The form drag contribution increases with Reynolds number from about 55% at Re_{in} = 100 to 85% at Re_{in} = 1300. The contribution of form drag is larger for the larger fin pitch because the flow is less

louver directed and there are larger pressure differentials between the top and bottom surface of the louvers.

SUMMARY AND CONCLUSIONS

High resolution time-dependent calculations are performed for two fin pitches (1.0 and 1.5) in a multilouvered geometry. Effect of fin pitch on general flow features, transition, heat transfer characteristics and friction are studied in a Reynolds number range of 100 to 1300. The following conclusions are made from this study.

a) For a given Reynolds number, the larger fin pitch results in smaller flow angles or less flow efficiency. For the two fin pitches studied here, the flow angles are nominally within 5 degrees of each other. The smaller flow angles associated with the larger fin pitch substantially increase the contribution of form drag to the total frictional losses.

b) In both cases flow instabilities appear in the exit wake at $Re_{in} = 400$. However, flow instabilities develop and spread in the interior of the array much faster for the larger fin pitch. Louver wake instabilities are the primary instability mechanism inside the array for the larger fin pitch, whereas leading edge shear layer instabilities are more dominant in the case of the smaller fin pitch.

c) Thermal wake effects play a substantial role in the heat transfer capability of individual louvers. These effects are much stronger for the smaller fin pitch.

d) For a given Reynolds number, the total heat transfer increases as the fin pitch increases due to the increased mass flow rate between fins. On the other hand, the heat transfer coefficient (Nusselt number based on mixed mean temperature) does not vary substantially between the two cases except in

the transitional and low Reynolds number range. The smaller fin pitch is much more effective for Reynolds numbers less than 200.

ACKNOWLEDGEMENTS

Dr. Zhang Xiaogang was supported by the Air Conditioning and Refrigeration Center (ACRC), Department of Mechanical and Industrial Engineering, University of Illinois at Urbana-Champaign.

NOMENCLATURE

b	fin thickness
A_c	minimum cross-sectional flow area
D_h	hydraulic diameter
f	Overall friction factor or frequency
F_p	fin pitch
h	convective heat transfer coefficient
j	Colburn factor
k	thermal conductivity
L_p	louver pitch
L_{xl}	length in x- direction used for representative pressure drop across fin
Nu	Nusselt number
P	pressure
p	pressure force *(P*area)*
Pr	Prandtl number
q	heat flux
Re	Reynolds number
S_2	length related to middle redirection louver
S_3	length related to entrance, exit, and redirection louver
S_4	length related to inlet and exit louver
t	time
T_{in}	temperature
T_f	fin temperature
T_{mean}	mixed mean temperature
T_{ref}	reference temperature
u,v	Cartesian velocity in x and y directions, respectively

u_{in} inlet velocity
$\vec{x}$ Physical space

Greek symbols
α mean flow angle
ν kinematic viscosity
θ louver angle (degrees)
ρ density of fluid
Ω surface area per unit depth

Superscripts

1 based on inlet temperature
2 based on mixed mean temperature
form denoting form drag
* dimensional quantities

Subscripts

f based on fin surface
fin based on whole multilouvered fin
in based on inlet
louv based on each louver

REFERENCES

1. Y. Chang, and C. Wang, A Generalized Heat Transfer Correlation for Louver Fin Geometry, *Int. J. Heat Mass Transfer*, Vol. **40**, No. **3**, pp. 533-544, 1997.
2. F. N. Beauvais, An Aerodynamic Look at Automobile Radiators, *SAE* Paper No. 65070, 1965.
3. C. J. Davenport, Heat Transfer and Flow Friction Characteristics of Louvered Heat Exchanger surfaces, *Heat Exchangers: Theory and Practice*, Taborek, J., Hewitt, G. F. and Afgan, N. (eds.), pp. 397-412, Hemisphere, Washington, D. C., 1983.
4. R. L. Webb, and P. Trauger, Flow Structure in the Louvered Fin Heat Exchanger Geometry, *Experimental Thermal and Fluid Science*, Vol. **4**, pp. 205-217, 1991.

5. A. Achaichia, and T. A. Cowell, Heat Transfer and Pressure Drop Characteristics of Flat tube and Louvered Plate Fin Surfaces, *Experimental Thermal and Fluid Science*, Vol. **1**, pp. 147-157, 1988.
6. A. Achaichia, and T. A. Cowell, A Finite Difference Analysis of Fully Developed Periodic Laminar Flow in Inclined Louvered Arrays, *Procs. 2nd UK National Heat Transfer Conference*, Glasgow, Vol. **2**, pp. 883-888, 1988.
7. K. Suga, H. Aoki, and T. Shingawa, Numerical Analysis on Two-Dimensional Flow and Heat Transfer of Louvered Fins Using Overlaid Grids, *JSM International Journal*, Vol. **33**, pp. 122-127, 1989.
8. K. Suga, and H. Aoki, Numerical Study on Heat Transfer and Pressure Drop in Multilouvered Fins, *ASME/JSME Thermal Engineering Proceedings*, Vol. **4**, pp. 361-368, 1991.
9. M. Hiramatsu, T. Ishimaru, and K. Matsuzaki, Research on Fins for Air Conditioning Heat Exchangers, *JSME International Journal*, Vol. **33**, pp. 749-756, 1990.
10. A. Achaichia, M. R. Heikal, Y. Sulaiman, and T. A. Cowell, Numerical Investigation of Flow and Friction in Louver Fin Arrays. *10th Int. Heat Transfer Conf., Heat Transfer 1994*, Vol. **4**, pp. 333-338, 1994.
11. W. P. Jones, and B. E. Launder, The Prediction of Laminarization with a Two-Equation Model of Turbulence, *Int. J. Heat Mass Transfer*, Vol. **15**, pp. 301-314, 1971.
12. L. W. Zhang, D. K. Tafti, F. M. Najjar, and S. Balachandar, Computations of Flow and Heat Transfer in Parallel-Plate Fin Heat Exchangers on the CM-5: Effects of Flow Unsteadiness and Three-Dimensionality, *Int. J. Heat Mass Transfer*, Vol. **40**, pp. 1325-1341, 1997.
13. L. W. Zhang, S. Balachandar, D. K. Tafti, and F. M. Najjar, Heat Transfer Enhancement Mechanisms in Inline and Staggered Parallel-Plate Fin Heat Exchangers, *Int. J. Heat Mass Transfer*, Vol. **40**, No. **10**, pp. 2307-2325, 1997.

14. D. K. Tafti, L. W. Zhang, and G. Wang, A Time-Dependent Calculation Procedure for Fully Developed and Developing Flow and Heat Transfer in Louvered Fin Geometries, in press *Numerical Heat Transfer*, submitted January 1998.

15. D. K. Tafti, G. Wang, and W. Lin, Flow Transition in a Multilouvered Fin Array, *submitted Int. J. Heat Mass Transfer*, September 1998.

16. F. H. Albernathy, and R. E. Kronauer, The formation of vortex streets, *J. Fluid Mech.*, **13**, pp.1-20, 1962.

17. P. W. Bearman, and D. M. Trueman, An investigation of the flow around rectangular cylinders, *Aero. Q.*, **23**, pp. 229-237, 1972.

18. J. C. Lane, and R. I. Loehrke, Leading edge separation from a blunt plate at low Reynolds number, Trans. ASME, *J. Fluids Eng.*, **102**, pp. 494-496, 1980.

19. D. K. Tafti, and S. P. Vanka, A three-dimensional numerical study of flow separation and reattachment on a blunt plate, *Physics of Fluids A*, **3**, pp. 2887-2909, 1991.

20. Y. Nakamura, Y. Ohya, and H. Tsuruta, Experiments on vortex shedding from flat plates with square leading and trailing edges, *J. Fluid Mech.*, **222**, pp. 437-447, 1991.

21. Y. Ohya, Y. Nakamura, S. Ozono, H. Tsuruta, and R. Nakayama, A numerical study of vortex shedding from flat plates with square leading and trailing edges, *J. Fluid Mech.*, **236**, pp. 445-460, 1992.

22. Y. Nakamura, T. Ohya, S. Ozono, and R. Nakayama, Experimental and numerical analysis of vortex shedding from elongated rectangular cylinders at low Reynolds numbers 200-10^3, *Journal of Wind Engineering and Industrial Aerodynamics*, **65**, pp. 301-308, 1996.

Table 1 Summary of non-dimensional geometrical parameters.

Case	F_p	θ	b	S_2	S_3	S_4
1	1.5	30	0.1	2.0	0.5	1.0
2	1.0	30	0.1	2.0	0.5	1.0

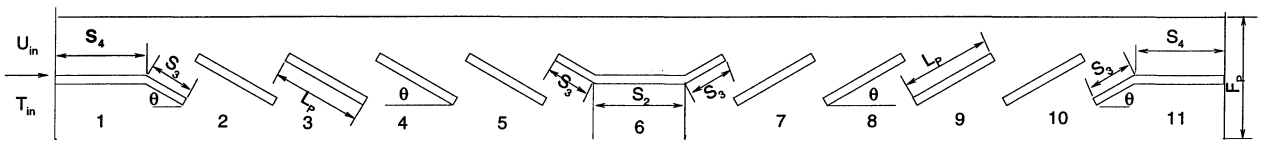

1(a)

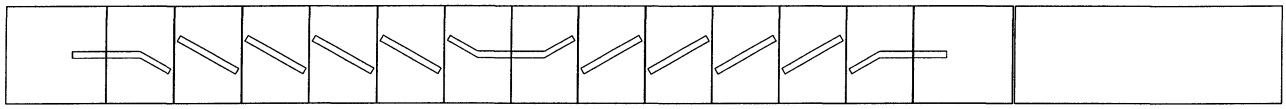

1(b)

Figure 1: (a) Multilouvered fin geometry ; (b) Multi-block computational domain.

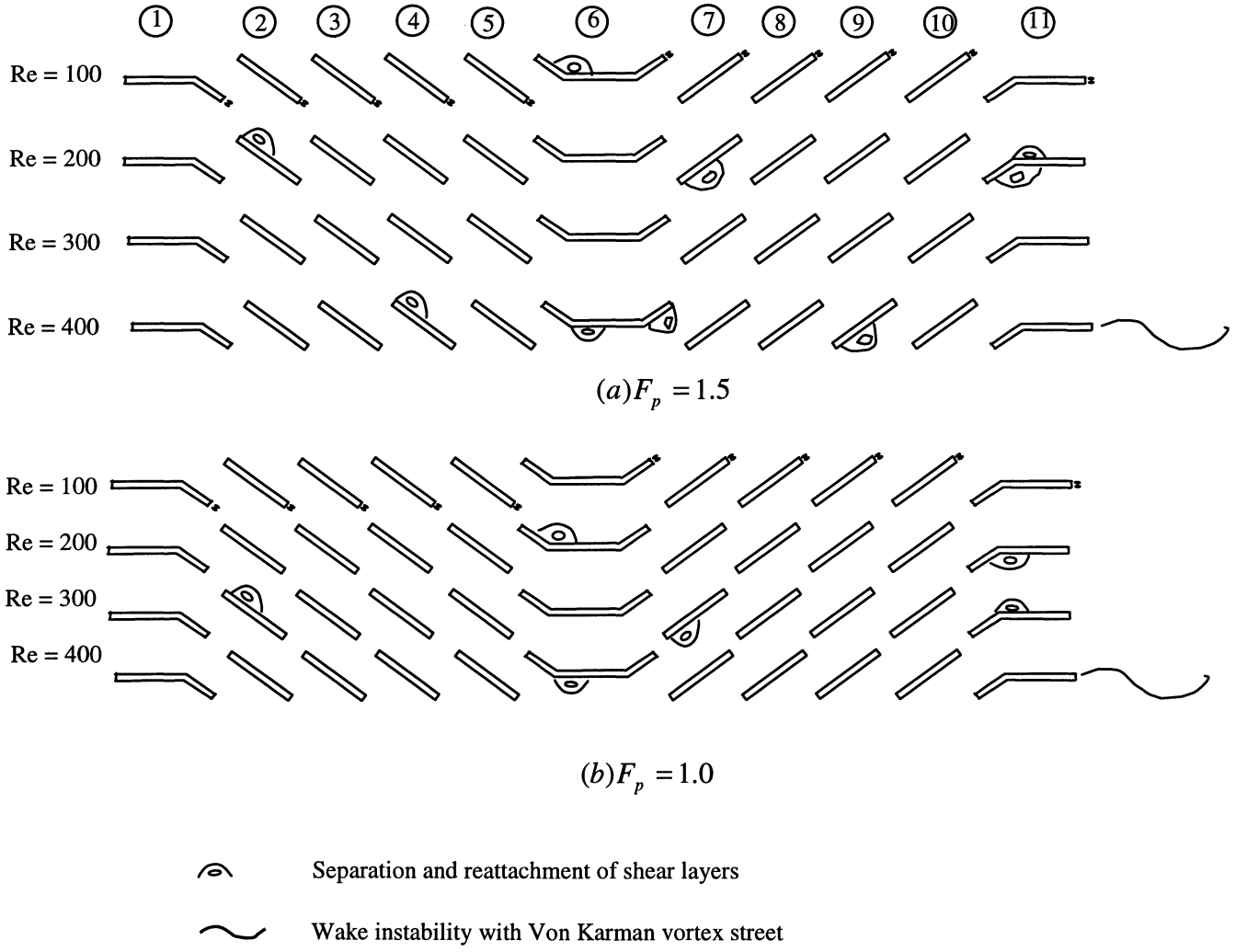

Figure 2: General flow features in the steady laminar regime. Only the initial appearance of flow features are represented

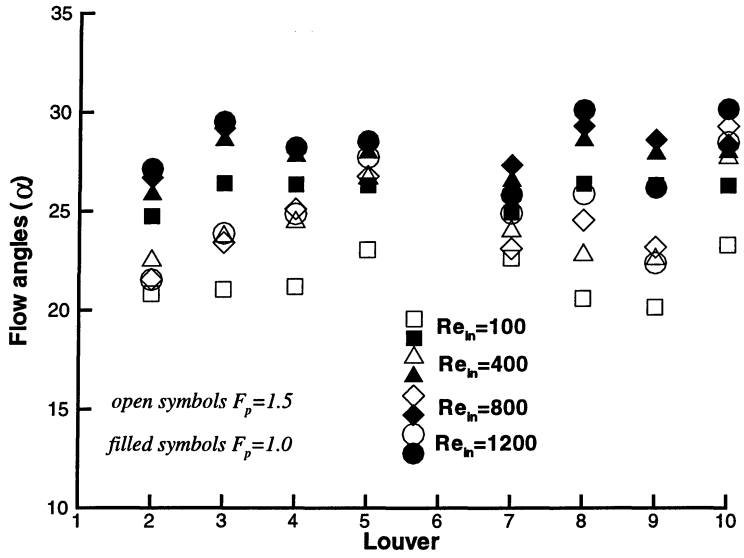

Figure 3: Calculated flow angles on a louver by louver basis.

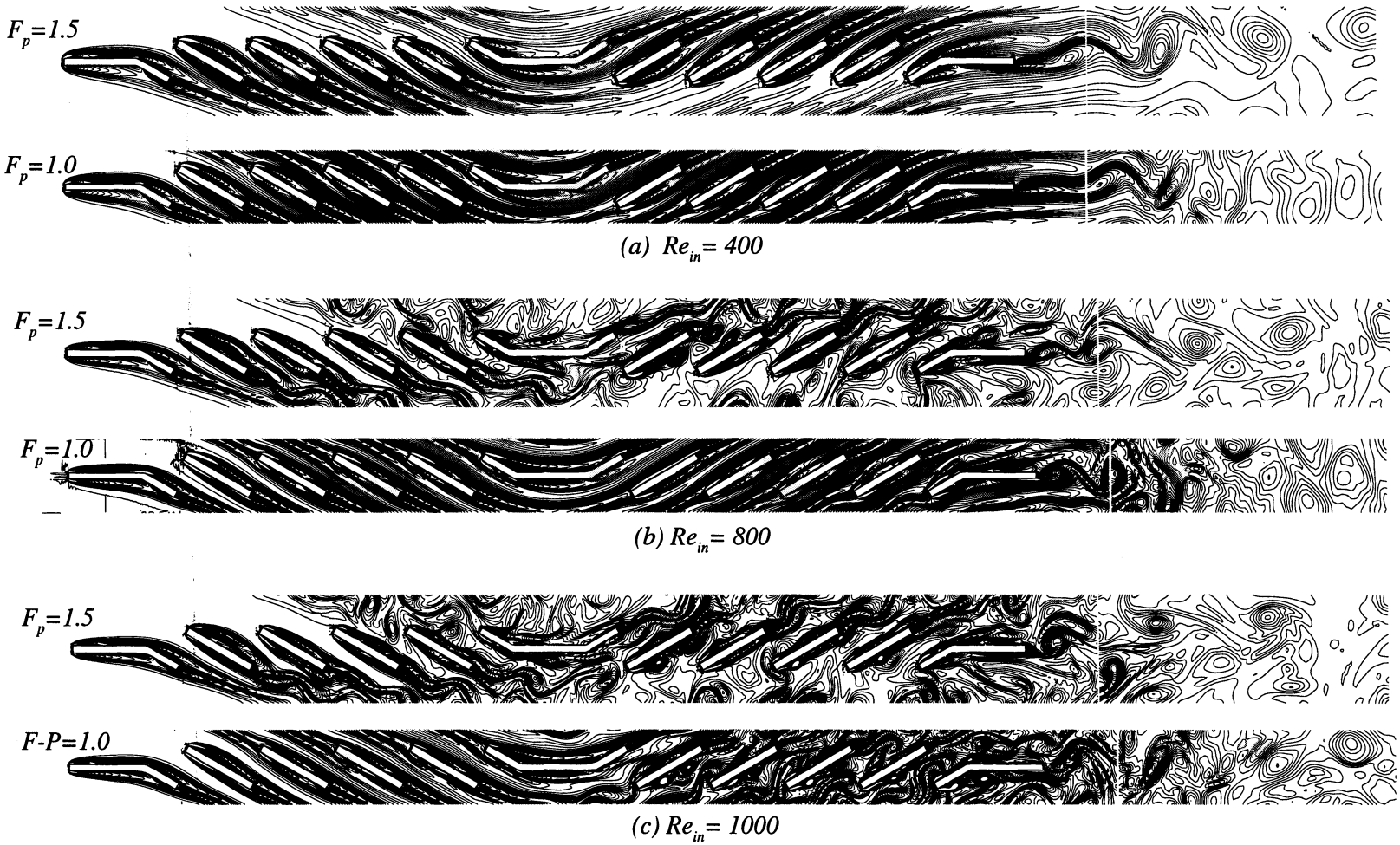

Figure 4: Instantaneous spanwise vorticity contours.

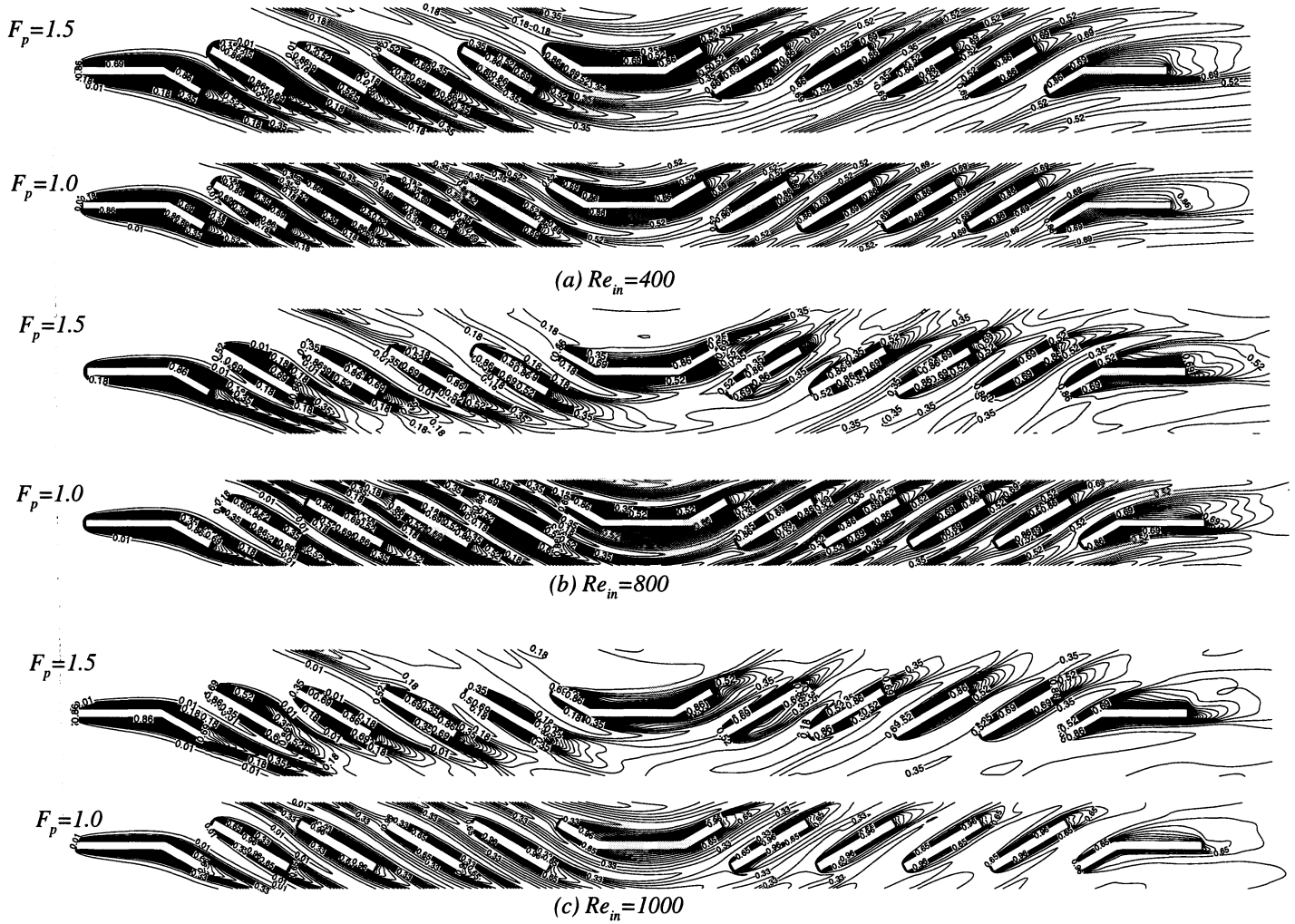

Figure 5: Time mean temperature contours.

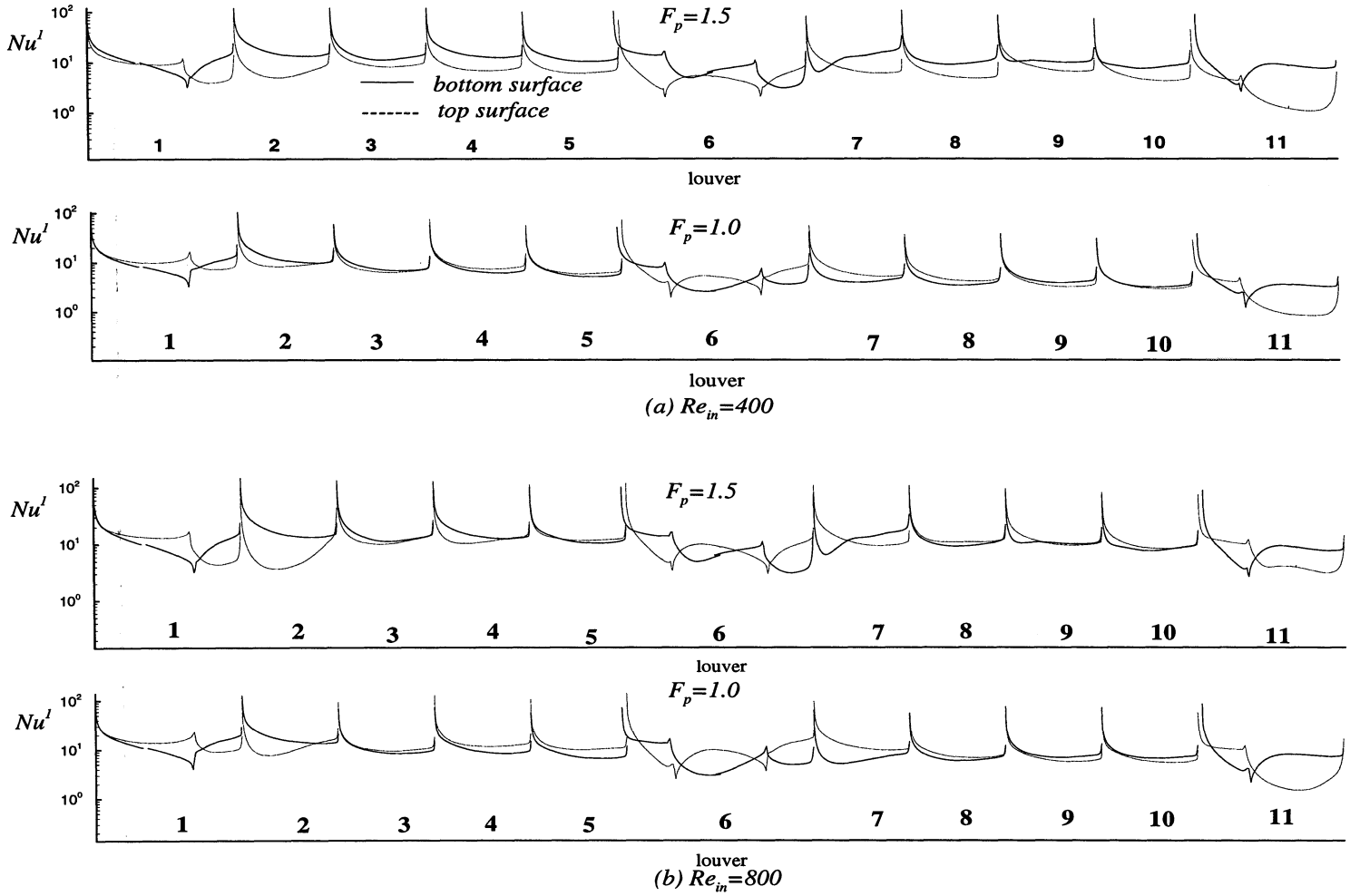

Figure 6: Local distribution of Nu^1 or heat flux (q).

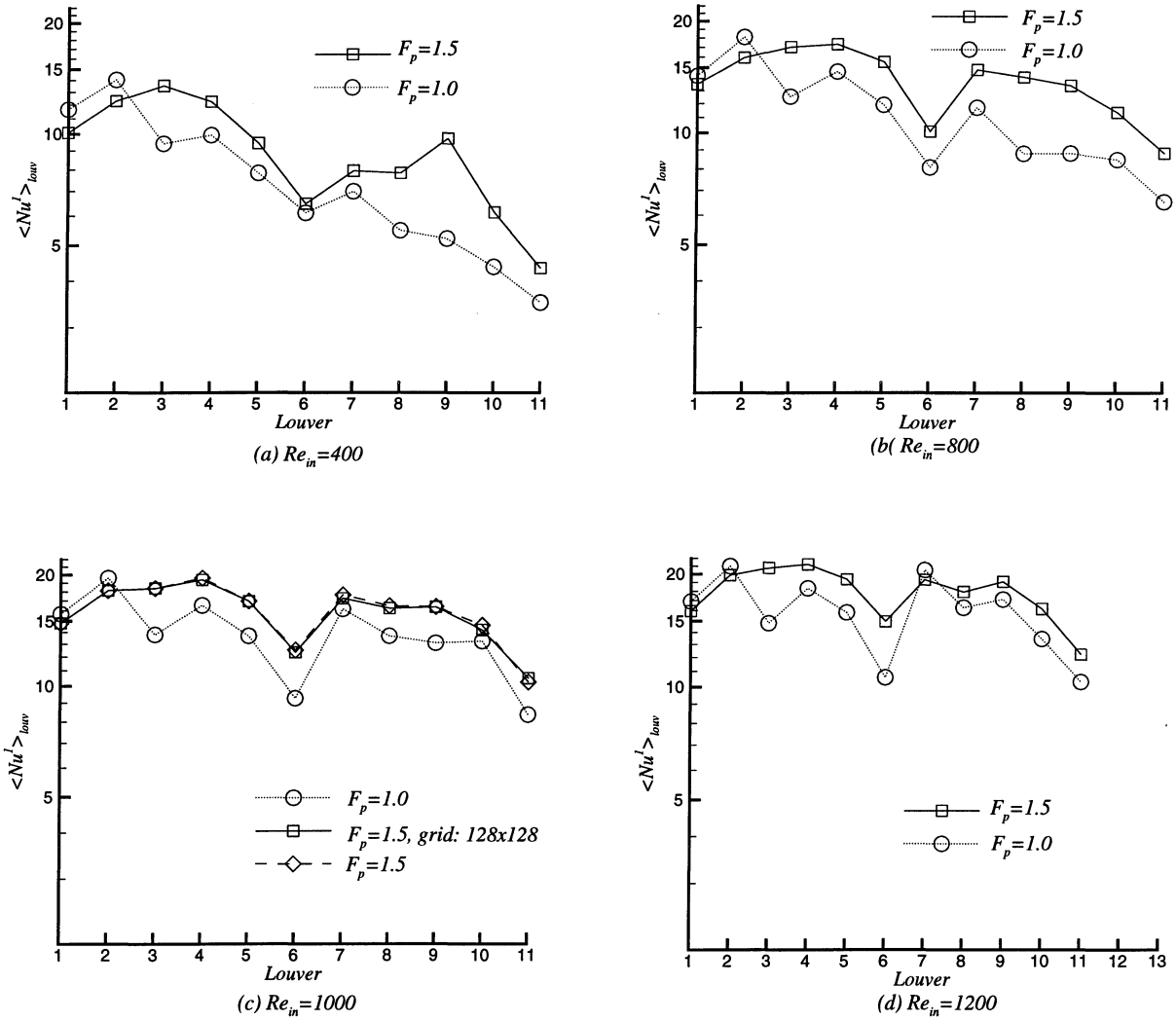

Figure 7: Louver by louver distribution of average Nusselt number, $< Nu^1 >_{louv}$ or average heat flux.

Fine grid results for Re_{in} = 1000 are also plotted to show grid independency.

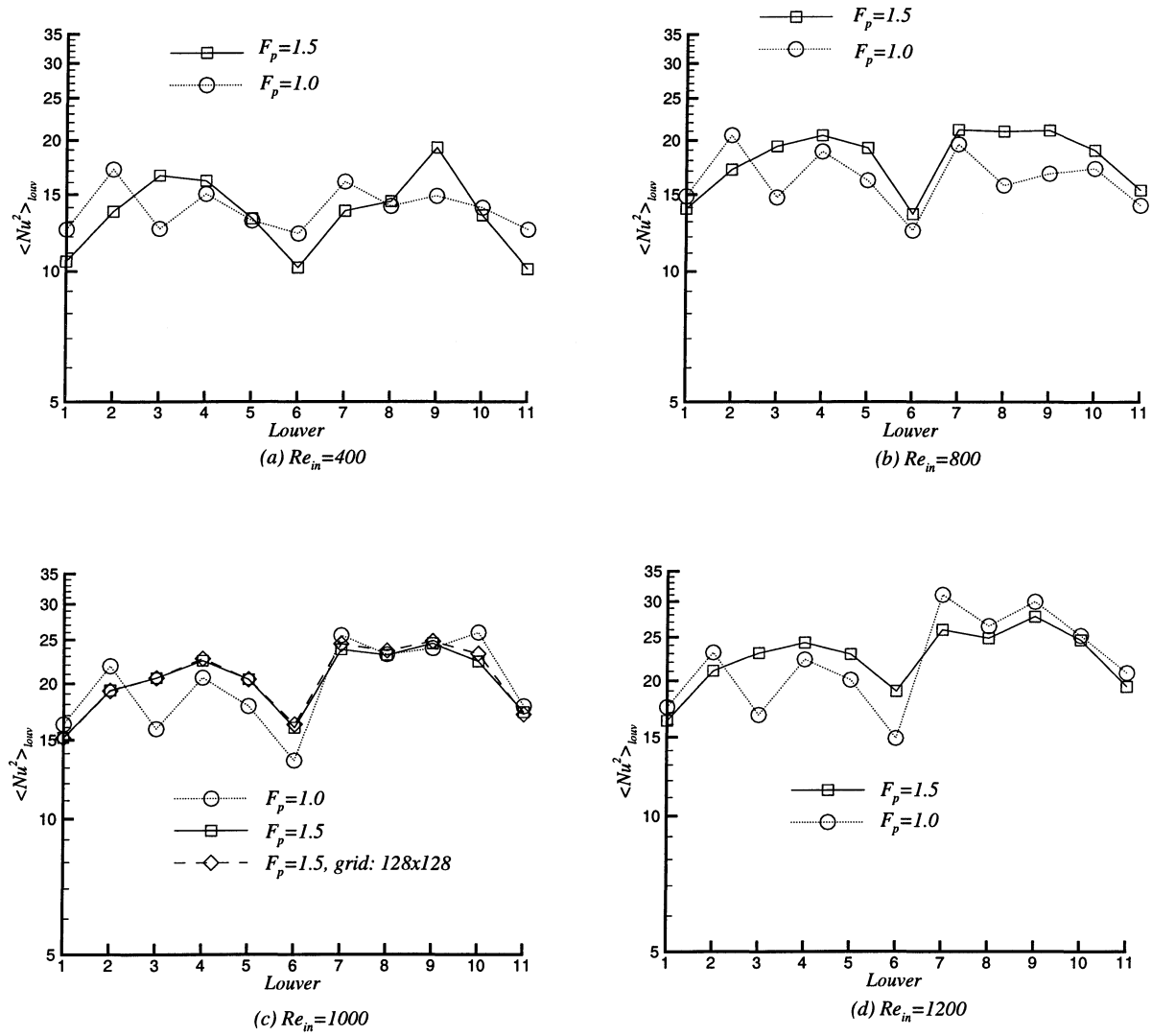

Figure 8: Louver by louver distribution of average Nusselt number based on mixed mean temperature, $< Nu^2 >_{louv}$. Fine grid results for Re_{in} = 1000 are also plotted to show grid independency.

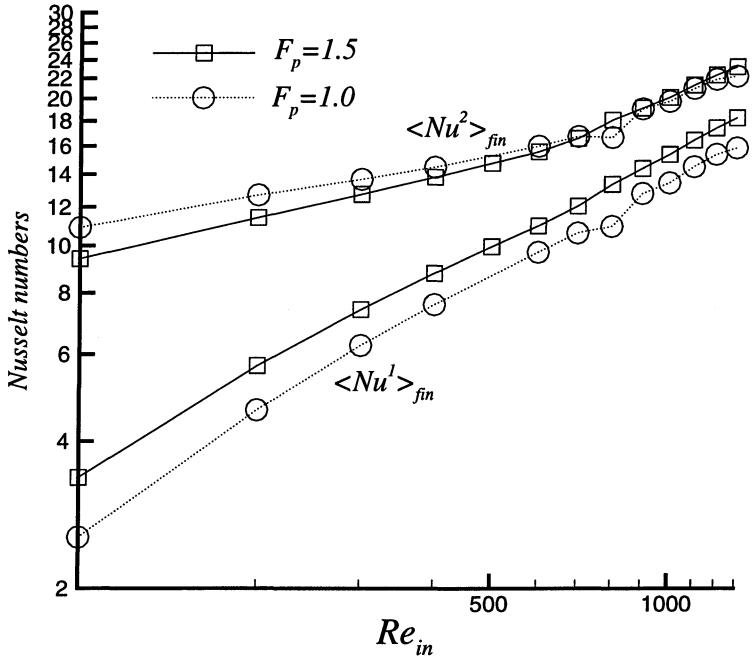

Figure 9: Variation of Nusselt number versus Reynolds number. $< Nu^1 >_{fin}$ represents the average heat flux, whereas $< Nu^2 >_{fin}$ represents the average heat transfer coefficient.

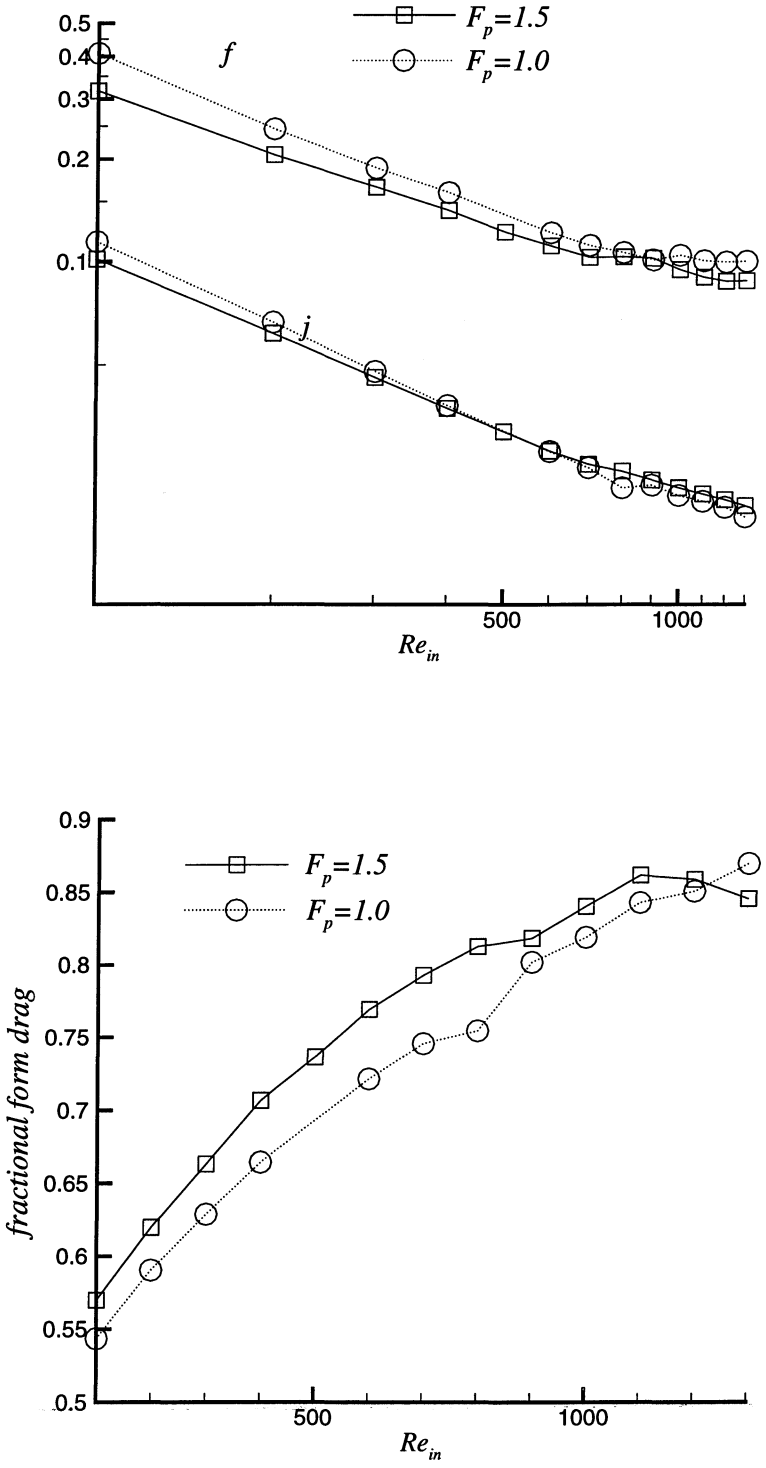

Figure 10: (a) Variation of friction factor and Colburn factor versus Reynolds number; (b) Fractional contribution of form drag to total pressure force.